

Electron-helium scattering in the S-wave model using exterior complex scaling

Daniel A. Horner,^{1,*} C. William McCurdy,^{2,3,1,†} and Thomas N. Rescigno^{2,‡}

¹*Department of Chemistry, University of California, Berkeley, California 94720*

²*Lawrence Berkeley National Laboratory, Chemical Sciences, Berkeley, California 94720*

³*Department of Applied Science, University of California, Davis, California 95616*

(Dated: June 16, 2004)

Electron-impact excitation and ionization of helium is studied in the S-wave model. The problem is treated in full dimensionality using a time-dependent formulation of the exterior complex scaling method that does not involve the solution of large linear systems of equations. We discuss the steps that must be taken to compute stable ionization amplitudes. We present total excitation, total ionization and single differential cross sections from the ground and $n = 2$ excited states and compare our results with those obtained by others using a frozen-core model.

I. INTRODUCTION

Since the early years of quantum mechanics and the development of scattering theory, an accurate description of the correlated motion of three unbound particles interacting via Coulomb forces has been a difficult problem to treat theoretically. Indeed, this problem was only reduced to computation in the last decade [1]. The difficulty stems from the long-range nature of the Coulomb potential which introduces a number of formal and practical complications. Although the formal theory of e-H ionization was developed in the 1960's by Peterkop [2] and by Rudge and Seaton [3, 4], it has not provided a practical path to computation. The asymptotic form of the wave function they derived is valid only in specific and limited geometries of the interacting particles and has proved to be too complicated to use as a boundary condition for solving the time-independent Schrödinger equation. Consequently, much of the work on electron-impact ionization has been carried out using perturbative, distorted-wave type methods or with close-coupling approaches that apply approximate two-body boundary conditions.

A practical path to accurate computation at low collision energies was only fully realized in the past few years. The key to overcoming the difficulties posed by the formal theory has been to formulate methods that do not rely on explicitly enforcing the boundary conditions for three-body Coulomb breakup. Several theoretical methods can be mentioned in this context. One such approach is the "time-dependent close-coupling" method developed by Pindzola, Schultz, Robicheaux and coworkers [5, 6]. In that approach, a wave packet is fired at the target atom and the time-dependent Schrödinger equation describing its dynamics is solved in a close-coupling formulation. Asymptotic boundary conditions are avoided since the time-dependent Schrödinger equation is solved as an ini-

tial value problem. Another successful method, which has been applied to the atomic double photoionization problem, is the hyperspherical R-matrix method with semi-classical outgoing waves [7]. In that approach, the time-independent Schrödinger equation is solved without detailed specification of three-body Coulomb boundary conditions by merging two different approaches: an R-matrix treatment of the entire system in the vicinity of the nucleus along with a semiclassical description of the evolution of the system in the asymptotic region. Exterior complex scaling (ECS) [8] avoids the explicit enforcement of boundary conditions entirely and has been successful in solving all aspects of the prototypical three-body Coulomb problem, electron-impact ionization of atomic hydrogen, to arbitrary accuracy [9, 10].

Most of the currently successful methods have been applied to study electron-impact ionization of multi-electron atoms by treating all but one active target electron in a frozen-core approximation, which reduces the problem to an effective three-body Coulomb system. The question we want to address here is whether the ECS method offers a practical approach to studying ionization of atoms with two *active* electrons. The method, as originally applied, involves solving large, sparse systems of linear equations. Extending this implementation, directly, to three electrons leads to linear systems that are extremely large and prohibitively expensive to solve. We have addressed that issue previously [11] by showing how the ECS method could be cast in a time-dependent formulation that scales more favorably with the number of electrons than the original time-independent formulation. The time-dependent ECS (TD-ECS) method was successfully applied to a problem involving four particles interacting via short range potentials.

Here we take the first steps toward applying ECS to the full electron-helium system. In this paper we extend the time-dependent ECS method to a system of four charged particles and consider the S-wave model of e^- -He ionization. The S-wave model provides a distillation of the full, 9-dimensional, problem into a system involving just three radial coordinates. While the problem we consider here is a model, it has the complexity of a true four-body Coulomb problem - involving long-range forces and

*dahorner@lbl.gov

†cwmccurdy@lbl.gov

‡tnrescigno@lbl.gov

an infinite number of two-body excitation channels - but simplifies the full problem by treating only states with zero angular momentum.

While the S-wave (or Temkin-Poet) model for e^- -H ionization has been a testbed for developing numerical approaches for studying ionization, the corresponding model for electron-helium scattering and ionization has received little attention in the literature, with most of the effort going towards solving the full electron-helium system under a number of approximations. Pindzola *et al.* [12] have used the time-dependent wave packet method to compute total cross sections with the S-wave model in the context of double ionization at high energies. This has been the only previous calculation to treat all of the electrons on the same footing, thus solving a true three-electron ionization problem. Plottke *et al.*, using the convergent close-coupling (CCC) method [13], have also reported results for this problem by freezing one of the electrons in the target. Under that approximation, the model is effectively equivalent to a two-electron system.

The method of exterior complex scaling is implemented here in 3D with a combined finite element-discrete variable representation (FEM-DVR)[14]. The FEM-DVR basis provides a numerical grid on which to perform the calculation, as well as an underlying expansion basis that allows the computed wave functions to be evaluated as a continuous function of the coordinates. ECS provides a method for computing a numerical representation of the physical scattering wave function on a finite volume by imposing only simple, outgoing-wave boundary conditions. Because of the simplified boundary conditions employed, the calculations do not automatically provide the desired scattering information. For the three-body problem, we have previously shown how to formulate a surface integral expression for the ionization amplitude that provides numerically stable and accurate cross sections on a finite volume [10, 15, 16]. With multi-electron targets, there are additional difficulties that arise which complicate the extraction of ionization amplitudes. The method we have devised for addressing these complications will be described as well.

The outline of this paper is as follows. The theory is presented in Section II. We begin with a description of the TD-ECS method for computing the scattered wave function. We then describe how this wave function is used in calculating amplitudes for excitation and ionization. The formal results are then applied in the case of the S-wave model. In Section III we present numerical results for excitation as well as total and differential ionization cross sections. In Section IV we summarize and discuss our findings.

II. THEORY

Our treatment of this problem involves two main parts: the computation of the three-electron scattering wave function and the extraction of physical cross sections.

A. Calculation of the scattered wave function

The starting point for all ECS applications is an equation that determines the purely outgoing part of the full wave function. To that end, we begin by partitioning the full wave function Ψ^+ into two parts:

$$\Psi^+ = \Phi_0 + \Psi_{\text{SC}}, \quad (1)$$

where the unperturbed function Φ_0 specifies the initial conditions and the scattered wave Ψ_{SC} contains only outgoing waves. Substituting Eq. (1) into the time-independent Schrödinger equation gives a driven equation for the scattered wave:

$$(E - H)\Psi_{\text{SC}} = (H - E)\Phi_0. \quad (2)$$

Eq. (2) must be solved with purely outgoing boundary conditions; the scattered wave Ψ_{SC} carries information about all the dynamical processes of interest.

The ECS method allows one to determine the scattered wave on a finite volume without having to detail its explicit asymptotic form. The method uses an analytic transformation where the electron coordinates are rotated into the complex plane beyond some point R_0 . This is accomplished by replacing each radial electron coordinate r with a scaled coordinate $R(r)$, defined by

$$R(r) = \begin{cases} r & r < R_0 \\ R_0 + (r - R_0)e^{i\theta} & r \geq R_0. \end{cases} \quad (3)$$

Purely outgoing functions decay on the complex portion of the coordinate $R(r)$. However, the function at distances less than R_0 are unaffected by the scaling. Thus, by requiring that solutions vanish at the origin and some appropriately large distance along the complex contour, we obtain a solution that is purely outgoing, and is effectively equal to the physical wave function on the real portion of the grid. The “effectively” qualifier reflects the fact that the interaction potentials on the r.h.s. of Eq. (2) must be truncated on the complex portions of the contour [1, 17]. As R_0 is increased, the solution approaches the exact physical scattered wave on the real portion of the grid. We note here that while the scattered wave is continuous along the contour defined by $R(r)$, its derivative is discontinuous at R_0 .

In most of the previous applications of ECS, Eq. (2) was solved by expanding the wave function on a grid using an appropriate discretization method (finite difference or finite elements) and solving the resulting linear equations to obtain the scattered wave solution. However, due to the poor scaling with respect of the number of particles, even in the case of three electrons, the size of the linear systems become very large and impractical to solve. Our strategy for circumventing this difficulty is to recast the problem with an equivalent time-dependent formulation [11] that does not require us to solve large linear systems and that scales favorably with increasing particle number.

In the reformulated method, the scattered wave function is computed as the Fourier transform of a time-dependent wavepacket,

$$\Psi_{\text{SC}} = -i \int_0^\infty e^{iEt} \chi(t) dt, \quad (4)$$

with

$$\chi(t) = e^{-iHt} \chi(0). \quad (5)$$

The initial “wavepacket” is simply given by

$$\begin{aligned} \chi(0) = \\ (H(R(r_1), R(r_2) \dots) - E) \Phi_0(R(r_1), R(r_2) \dots). \end{aligned} \quad (6)$$

This formulation follows from noting that the solution of Eq. (2) which we seek can be formally written as

$$\Psi_{\text{SC}} = G^+ \chi(0), \quad (7)$$

with G^+ being the full Green’s function

$$\begin{aligned} G^+ &= (E - H + i\epsilon)^{-1} \\ &\underset{\epsilon \rightarrow 0}{=} \frac{1}{i} \int_0^\infty e^{i(E+i\epsilon)t} e^{-iHt}. \end{aligned} \quad (8)$$

Because we are using ECS, the wavepacket $\chi(t)$ will limit to zero for large $\{r_i\}$ as $t \rightarrow \infty$, so the $+i\epsilon$ in Eq. (8) can be dropped. Eq. (4) is thus formally equivalent to the solution of Eq. (2). Instead of solving large linear systems, it requires that we propagate $\chi(0)$ on the ECS contour in multiple dimensions for times sufficiently large to converge the Fourier transform that provides the numerical representation of Ψ_{SC} .

We seek a method that scales well with particle number and therefore one that does not involve solutions of linear equations representing multiple dimensions at each time step. To that end, we employ a split operator approximation [18] for the time propagation operator. The Hamiltonian for d particles is first separated into one-two-body terms:

$$\begin{aligned} H &= \sum_{i=1}^d h_1(r_i) + \sum_{i>j=1}^d v_2(r_i, r_j) \\ &\equiv H_1 + V_2, \end{aligned} \quad (9)$$

and the propagator is then approximated as

$$\begin{aligned} e^{-iH\Delta t} &\approx \exp \left[-i \left(\frac{\Delta t}{2} \right) V_2 \right] \\ &\times \left[\prod_{i=1}^d e^{-ih_1(r_i)\Delta t} \right] \exp \left[-i \left(\frac{\Delta t}{2} \right) V_2 \right]. \end{aligned} \quad (10)$$

To approximate the one-body Hamiltonian terms, we use a second-order Crank-Nicolson propagator,

$$\begin{aligned} e^{-ih_1\Delta t} &\approx \left(1 + ih_1 \frac{\Delta t}{2} - h_1^2 \frac{\Delta t^2}{12} \right)^{-1} \\ &\times \left(1 - ih_1 \frac{\Delta t}{2} - h_1^2 \frac{\Delta t^2}{12} \right). \end{aligned} \quad (11)$$

The scaling properties of this propagator depend on the representations of the operators, which we have yet to specify. Earlier implementations of ECS used finite difference methods, but in the present work we employ, for each radial electron coordinate, the combined finite element-discrete variable representation (FEM-DVR) introduced by Rescigno and McCurdy [14]. The DVR combines a high-order polynomial treatment of the kinetic energy operator with the advantage of a diagonal representation of any local potential operator. For the DVR representation, we use a basis of so-called “Lobatto shape functions” [19], which are Lagrange interpolating polynomials with mesh points derived from a Gauss-Lobatto quadrature. Gauss-Lobatto quadrature is similar to the more familiar Gauss-Legendre quadrature, with the difference that in Gauss-Lobatto quadrature two of the points are constrained to coincide with the specified end-points. Since Gauss-Lobatto quadrature explicitly includes the end-points as quadrature points, it is possible to combine this particular variety of DVR with the finite-element method, as outlined in ref. [14]. Moreover, by choosing one of the element boundaries to coincide with the point R_0 where the real and complex parts of the ECS contour join, the derivative discontinuity in the wave function at R_0 is handled exactly.

With the FEM-DVR, matrix element computation is greatly simplified compared with other basis set methods. When the integrals are approximated using the underlying Gauss quadrature, the local potential operators have a diagonal representation. Matrix elements of derivative operators, such as the kinetic energy, are not diagonal, but are given by simple analytic formulas. With FEM-DVR, the kinetic energy operator has a blocked matrix structure, where each block representing a particular finite element is full, and the various blocks are connected by the end-point DVR functions that join adjacent elements [14]. Thus the overall kinetic energy matrix, while not diagonal, can be very sparse, depending on the number of elements and order of quadrature used in each element.

The efficiency of the time-dependent formulation in more than two dimensions becomes readily apparent with an FEM-DVR representation. Since the matrix elements of local functions are diagonal and the one body Hamiltonian terms separate, the number of operations needed to evaluate the exponential propagators in Eq. (10) can be easily estimated. Assume we have n grid points in each of d dimensions. For one time step, each operation on the wave packet with $\exp(-iV_2\Delta t/2)$ requires one multiplication per grid point, or of order n^d operations. The operator $\exp(-ih_1\Delta t)$ in each dimension can be represented by an $n \times n$ matrix (Eq. (11)) that need be computed only once. Each operation with $\exp(-ih_1\Delta t)$ involves a matrix multiply for one of the dimensions that has to be done for each point in the other dimensions, and thus requires of the order $n^2 \times n^{d-1} = n^{d+1}$ elementary operations. The entire propagator thus requires of order $2n^d + dn^{d+1} \sim dn^{d+1}$ operations per time step. If

we attempted to represent the time-independent driven Schrödinger equation on the $n^d \times n^d$ grid, we would have to solve a sparse set of linear equations for Ψ_{SC} . If iterative methods were used, which offer the best scaling with n , the effort required would scale no better than n^{2d} . The scaling advantage of the time-dependent approach implemented here is that of n^{d+1} versus n^{2d} . For $d = 3$ and $n = 150$, which is typically required in these calculations, that advantage is 5×10^8 vs. 10^{13} operations to perform.

B. Extracting cross sections

The formal and computational advantage of ECS is that it does not make reference to any specific asymptotic boundary conditions other than the requirement that the scattered wave be purely outgoing. Once the scattered wave has been calculated, we must decide how to extract the detailed dynamical information it describes. One would not normally view this as a major issue, since in most standard methods, the asymptotic boundary conditions that define the dynamical quantities of interest are used in the generation of the wave function. But in the ECS method, what is obtained is a numerical representation of a wave function that contains information about all processes that are allowed at a specific total energy, as detailed specification of scattering boundary conditions is avoided by design.

A simple and straight-forward way to obtain the ionization cross section is to compute the quantum mechanical flux through a surface that lies inside the region where the coordinates are real. While this method was used in the first successful applications of ECS to e-H ionization [9, 20], there are intrinsic problems with this approach. The method requires fairly large grids since the numerically computed quantities must be extrapolated to infinite grid size, where the flux can be related to the differential cross sections for ionization. More serious is the problem that the grids must be large enough to allow the physical region inhabited only by the ionization portion of the scattered wave to be distinguishable from the parts that describe discrete two-body channels. The requirement that the ionization wave be “uncovered” before the asymptotic flux is calculated can require grids that extend well beyond the range where the interaction potentials are appreciable.

The most practical, and economical, approach to calculating both excitation and breakup cross sections is to formulate the problem in terms of integral expressions for the underlying scattering amplitudes [15]. For discrete excitations in the present case of a three-electron radial problem, we can begin with the formal expression

$$f_{i \rightarrow n} = \frac{2}{\sqrt{k_n}} \langle \phi_n(r_1, r_2) \sin(k_n r_3) | E - H_1 | \Psi^+ \rangle, \quad (12)$$

where ϕ_n is a discrete target state and H_1 is the unperturbed Hamiltonian corresponding to the incident chan-

nel arrangement, so that:

$$(H_1 - E) |\phi_n(r_1, r_2) \sin(k_n r_3)\rangle = 0. \quad (13)$$

It is to be understood that the matrix element in Eq. (12), and in all the expressions that follow, is carried out over a finite volume defined by some hyperradius where the electron coordinates are all real. We can then use Green’s theorem, along with Eq. (13), to express the amplitude as a surface integral:

$$\begin{aligned} f_{i \rightarrow n} &= \frac{1}{\sqrt{k_n}} \int_S [\phi_n(r_1, r_2) \sin(k_n r_3) \nabla \Psi^+(r_1, r_2, r_3) \\ &\quad - \Psi^+(r_1, r_2, r_3) \nabla \phi_n(r_1, r_2) \sin(k_n r_3)] \cdot d\hat{\mathbf{S}} \\ &= \frac{1}{\sqrt{k_n}} \int_S [\phi_n(r_1, r_2) \sin(k_n r_3) \nabla \Psi_{\text{SC}}(r_1, r_2, r_3) \\ &\quad - \Psi_{\text{SC}}(r_1, r_2, r_3) \nabla \phi_n(r_1, r_2) \sin(k_n r_3)] \cdot d\hat{\mathbf{S}} \end{aligned} \quad (14)$$

where the replacement of Ψ^+ by Ψ_{SC} in the surface integral follows from an examination of the integrand of Eq. (14) on the surface.

The derivation of a workable formula for the ionization amplitude requires some care. We preface this discussion by noting that all of the matrix elements considered here are presumed to be evaluated on a large but finite volume, so we will employ the standard rearrangement theory for short-ranged interactions and not address any of the difficulties posed by the formal theory of ionization. The connection with the formal theory, and in particular the question of the proper definition of the overall phase of the ionization amplitude, which does not affect any physical cross section, has been discussed at length elsewhere and will not be repeated here [16, 21].

We have previously pointed out that, for a one-electron target, the following expression for the breakup amplitude [15],

$$f(k_1, k_2) = 2 \langle \sin(k_1 r_1) \sin(k_2 r_2) | E - T | \Psi_{\text{SC}} \rangle, \quad (15)$$

where T is the total kinetic energy operator, while formally correct, does not prove to be useful in an actual numerical calculation on a finite volume. This failure can be traced to the contribution of discrete two-body channels in Ψ_{SC} which give rise to overlap terms that properly converge to Dirac δ functions only for infinite volumes. This contamination of the ionization amplitude from bound states renders Eq. (15) useless on a finite volume. The solution to this problem is to employ a formally equivalent expression with distorted waves in the final state:

$$f(k_1, k_2) = 2 \langle \varphi_{k_1} \varphi_{k_2} | E - T - V_1 | \Psi_{\text{SC}} \rangle, \quad (16)$$

where V_1 is the distorted wave potential corresponding to the final state. In the e^- -H case, for example, we choose the distorted waves to be Coulomb functions with $Z = 1$ [16]. Since the Coulomb functions are eigenfunctions of the same Hamiltonian as the hydrogenic bound states, orthogonality is realized on the finite volume and

the spurious contributions to the breakup amplitude are eliminated.

The natural extension of Eq. (16) to the present helium case, for single ionization leaving the ion in the n -th excited state, would be

$$f(k_1, k_2) = 2 \langle \varphi_n \varphi_{k_1} \varphi_{k_2} | E - T - V_1 | \Psi_{\text{SC}} \rangle. \quad (17)$$

But now the use of distorted waves alone cannot completely eliminate the contamination of the ionization amplitude by discrete excitation channels, since there is generally no orthogonality relationship between the single-particle distorted waves and the exact two-particle bound states of the target. Nevertheless, we can still achieve much by choosing the distorted wave potential judiciously. The excited states of the model S-wave helium atom, both singlet and triplet, are reasonably well described by single-configuration wave functions of the form ${}^{1,3}|\varphi_{1s}\varphi_{ns}\rangle$, where φ_{1s} is the $1s$ orbital of He^+ . The φ_{ns} orbitals for the corresponding singlet and triplet states are of course not identical, but they are reasonably similar. With these considerations in mind, we choose the distorted waves to be solutions of the triplet static-exchange equation,

$$\left(T - \frac{2}{r} + J_{1s} - K_{1s} - k^2/2\right)\varphi_k = 0, \quad (18)$$

where J_{1s} and K_{1s} are the usual Coulomb and exchange operators constructed with the He^+ $1s$ orbital. Note that the He^+ $1s$ orbital is an eigenfunction of this equation, as are the triplet φ_{ns} orbitals. This choice therefore guarantees *approximate* orthogonality between the distorted waves and *all* the excited helium target states. It does *not*, however, eliminate contamination of the breakup amplitude by the ground-state channel, since the neutral helium ground-state $1s$ orbital is very different from the He^+ $1s$ orbital.

To address the problem of contamination by the elastic channel, and to further improve on the prescription for computing a stable ionization amplitude, we employ the technique of ‘‘asymptotic subtraction’’ which we introduced in our earlier study of breakup with short-ranged potentials [11]. The idea is to try to remove the asymptotic contribution of the discrete two-body channels to the scattered wave before computing the ionization amplitude. Asymptotically, the scattered wave has the form

$$\Psi_{\text{SC}} = \Psi_{\text{SC}}^{\text{ion}} + \sum_n \left(\frac{f_{i \rightarrow n}}{\sqrt{k_n}} \right) \phi_n(r_1, r_2) e^{ik_n r_3}. \quad (19)$$

So by subtracting the sum that appears in Eq. (19) from Ψ_{SC} we can, in principle, isolate, asymptotically, the pure ionization portion of the scattered wave. The excitation amplitudes $f_{i \rightarrow n}$ can be calculated using Eq. (12) or (14). There are of course an infinite number of discrete two-body channels, but on a finite volume only a finite number of bound states can be supported.

The ionization amplitude is thus evaluated by starting with the expression

$$f(k_1, k_2) = 2 \langle \varphi_n \varphi_{k_1} \varphi_{k_2} | E - T - V_1 | \Psi_{\text{SC}}^{\text{ion}} \rangle, \quad (20)$$

and using Green’s theorem to convert it to a surface integral

$$f(k_1, k_2) = \int_S [\varphi_n(r_1)\varphi_{k_1}(r_2)\varphi_{k_2}(r_3)\nabla\Psi_{\text{SC}}^{\text{ion}}(r_1, r_2, r_3) - \Psi_{\text{SC}}^{\text{ion}}(r_1, r_2, r_3)\nabla\varphi_n(r_1)\varphi_{k_1}(r_2)\varphi_{k_2}(r_3)] \cdot \hat{\mathbf{n}} dS. \quad (21)$$

The use of the surface integral form of the amplitude, which only depends of the asymptotic part of the scattered wave, is now essential, since asymptotic subtraction changes the interior part of the scattered wave and makes the volume integral representation of the amplitude invalid. We have found that asymptotic subtraction and the correct choice of distorted waves are both essential in computing accurate ionization cross sections.

C. S-Wave model of helium

As we have mentioned, the S-wave model arises from retaining only the first, $l = 0$, term in the angular momentum expansion of the electron repulsion potentials. The full Hamiltonian for the e^- -He system in the S-wave model is

$$H(r_1, r_2, r_3) = T_1 + T_2 + T_3 - \frac{2}{r_1} - \frac{2}{r_2} - \frac{2}{r_3} + \frac{1}{r_{>(1,2)}} + \frac{1}{r_{>(1,3)}} + \frac{1}{r_{>(2,3)}}, \quad (22)$$

where $r_{>(1,2)} = \max(r_1, r_2)$.

The helium target bound states $\phi_n(r_1, r_2)$ are eigenfunctions of the 2-electron Hamiltonian,

$$H_t(r_1, r_2)\phi_n(r_1, r_2) = \left[T_1 + T_2 - \frac{2}{r_1} - \frac{2}{r_2} + \frac{1}{r_{>(1,2)}} \right] \phi_n(r_1, r_2) = E_n \phi_n(r_1, r_2). \quad (23)$$

The spatial part of these states can be either symmetric or anti-symmetric with respect to interchange of the two electron coordinates, corresponding to singlet, $s_n = 0$, or triplet, $s_n = 1$, spin-coupling of the target electrons.

The initial conditions for determining Ψ_{SC} are contained in the specification of Φ_0 : since the full Hamiltonian is totally symmetric, the permutational properties of Ψ_{SC} are set by the initial wave function. To construct a physical three-electron initial state, labeled by target state n and spin s_n and total spin ($S = 1/2$ or $S = 3/2$), we can apply the antisymmetrization operator to the product of a three-electron spin state, $|S, s_n\rangle$, and an unperturbed spatial function,

$$\Phi_0^{n, S, s_n}(r_1, r_2, r_3) = \mathcal{A} \left[\phi_n(r_1, r_2) \frac{\sin(k_n r_3)}{\sqrt{k_n}} |S, s_n\rangle \right]. \quad (24)$$

For example, the three electron doublet spin eigenfunction ($S = 1/2$) for a triplet target state ($s_n = 1$) is

$$\left|\frac{1}{2}, 1\right\rangle = \frac{1}{\sqrt{6}}(2\alpha\alpha\beta - \alpha\beta\alpha - \beta\alpha\alpha), \quad (25)$$

where we have chosen the projection $m_S = \frac{1}{2}$. For the fully antisymmetric three-electron state, the spatial and spin portions of the wave function generally do not factor.

Having defined the unperturbed initial state with Eq. (24), we must construct a solution of the driven Schrödinger for the corresponding scattered wave, Ψ_{SC}^{n,S,s_n} :

$$(E - H)\Psi_{SC}^{n,S,s_n} = (H - E)\Phi_0^{n,S,s_n} \quad (26)$$

In practice, it is only necessary to solve this equation for a single arrangement of the electron coordinates since any other arrangement can be obtained by an appropriate permutation of electron coordinate labels, i.e., we can propagate an unsymmetric initial state and then construct the desired physical state by combining the solution vectors with different permutations of the coordinate indices. The single arrangement we compute is

$$(E - H)\psi_i(r_1, r_2, r_3) = (H - E)\phi_{n_i}(r_1, r_2) \frac{\sin(k_i r_3)}{\sqrt{k_i}}. \quad (27)$$

The amplitudes for discrete excitation, $F_{i \rightarrow f}^{S,s_f,s_i}$, can then be constructed from the quantities:

$$\begin{aligned} f_{fi}^{(1)} &= 2 \left\langle \phi_{n_f}(r_1, r_2) \frac{\sin(k_f r_3)}{\sqrt{k_f}} \left| E - H_0^{123} \right| \psi_i(r_1, r_2, r_3) \right\rangle \\ f_{fi}^{(2)} &= 2 \left\langle \phi_{n_f}(r_2, r_3) \frac{\sin(k_f r_1)}{\sqrt{k_f}} \left| E - H_0^{231} \right| \psi_i(r_1, r_2, r_3) \right\rangle \\ f_{fi}^{(3)} &= 2 \left\langle \phi_{n_f}(r_3, r_1) \frac{\sin(k_f r_2)}{\sqrt{k_f}} \left| E - H_0^{312} \right| \psi_i(r_1, r_2, r_3) \right\rangle, \end{aligned} \quad (28)$$

where $H_0^{ijk} = H_t(r_i, r_j) + T_k$. Using Green's identities, as discussed above, these matrix elements can be converted to surface integrals. For example,

$$\begin{aligned} f_{fi}^{(1)} &= \frac{1}{\sqrt{k_f}} \int_S [\phi_{n_f}(r_1, r_2) \sin(k_f r_3) \nabla \psi_i(r_1, r_2, r_3) \\ &\quad - \psi_i(r_1, r_2, r_3) \nabla \phi_{n_f}(r_1, r_2) \sin(k_f r_3)] \cdot \hat{\mathbf{n}} dS. \end{aligned} \quad (29)$$

These arrangement amplitudes are not entirely independent. In fact, $f_{fi}^{(2)} = \pi_i \pi_f f_{fi}^{(3)}$, where $\pi_n = (1 - 2s_n)$

is the parity of target state n . The arrangement amplitudes are combined to obtain the physical amplitudes $F_{i \rightarrow f}^{S,s_f,s_i}$. Table I gives explicit formulas for the various physical amplitudes in terms of the arrangement amplitudes, based on the initial and final spin states of the three electrons. The physical cross sections for inelastic scattering are computed using

$$\sigma_{fi} = \frac{2S + 1}{2(2s_i + 1)} \left(\frac{4\pi}{k_i^2} \right) \left| F_{i \rightarrow f}^{S,s_f,s_i} \right|^2. \quad (30)$$

$ S, s_i\rangle$	$ S, s_f\rangle$	$F_{i \rightarrow f}^{S,s_f,s_i}$
$ \frac{1}{2}, 0\rangle$	$ \frac{1}{2}, 0\rangle$	$\frac{1}{2} [2f_{fi}^{(1)} - f_{fi}^{(2)} - f_{fi}^{(3)}]$
$ \frac{1}{2}, 0\rangle$	$ \frac{1}{2}, 1\rangle$	$\frac{\sqrt{3}}{2} [f_{fi}^{(3)} - f_{fi}^{(2)}]$
$ \frac{1}{2}, 1\rangle$	$ \frac{1}{2}, 0\rangle$	$\frac{\sqrt{3}}{2} [f_{fi}^{(2)} - f_{fi}^{(3)}]$
$ \frac{1}{2}, 1\rangle$	$ \frac{1}{2}, 1\rangle$	$\frac{1}{2} [2f_{fi}^{(1)} - f_{fi}^{(2)} - f_{fi}^{(3)}]$
$ \frac{3}{2}, 1\rangle$	$ \frac{3}{2}, 1\rangle$	$f_{fi}^{(1)} + f_{fi}^{(2)} + f_{fi}^{(3)}$

TABLE I: Expressions for scattering and ionization amplitudes in terms of individual arrangement amplitudes.

For the single ionization amplitudes, similar considerations apply. Following the discussion of Sec. IIB, we begin by using asymptotic projection to isolate the ionization portion of the scattered wave for a single arrangement:

$$\begin{aligned} \psi_i^{\text{ion}}(r_1, r_2, r_3) &= \psi_i(r_1, r_2, r_3) \\ &\quad - \sum_n \frac{1}{\sqrt{k_n}} \left(f_{ni}^{(1)} \phi_n(r_1, r_2) e^{ik_n r_3} \right. \\ &\quad \left. + f_{ni}^{(2)} \phi_n(r_2, r_3) e^{ik_n r_1} \right. \\ &\quad \left. + f_{ni}^{(3)} \phi_n(r_3, r_1) e^{ik_n r_2} \right). \end{aligned} \quad (31)$$

Note that the scattered wave corresponding to a single initial arrangement has asymptotic two-body channel components in all arrangements, each of which must be removed in computing ψ_i^{ion} .

For the single ionization amplitudes, the final states are assembled from products of a He^+ orbital φ_n and two continuum distorted waves φ_{k_1} and φ_{k_2} . As in the case of excitation, we can define different arrangement amplitudes from which the physical ionization amplitudes can be assembled:

$$\begin{aligned}
f_{fi}^{(1)}(k_1, k_2) &= 2 \langle \varphi_n(r_1) \varphi_{k_1}(r_2) \varphi_{k_2}(r_3) | E - H_0 | \psi_i^{\text{ion}}(r_1, r_2, r_3) \rangle \\
f_{fi}^{(2)}(k_1, k_2) &= 2 \langle \varphi_n(r_2) \varphi_{k_1}(r_3) \varphi_{k_2}(r_1) | E - H_0 | \psi_i^{\text{ion}}(r_1, r_2, r_3) \rangle \\
f_{fi}^{(3)}(k_1, k_2) &= 2 \langle \varphi_n(r_3) \varphi_{k_1}(r_1) \varphi_{k_2}(r_2) | E - H_0 | \psi_i^{\text{ion}}(r_1, r_2, r_3) \rangle.
\end{aligned}$$

(32)

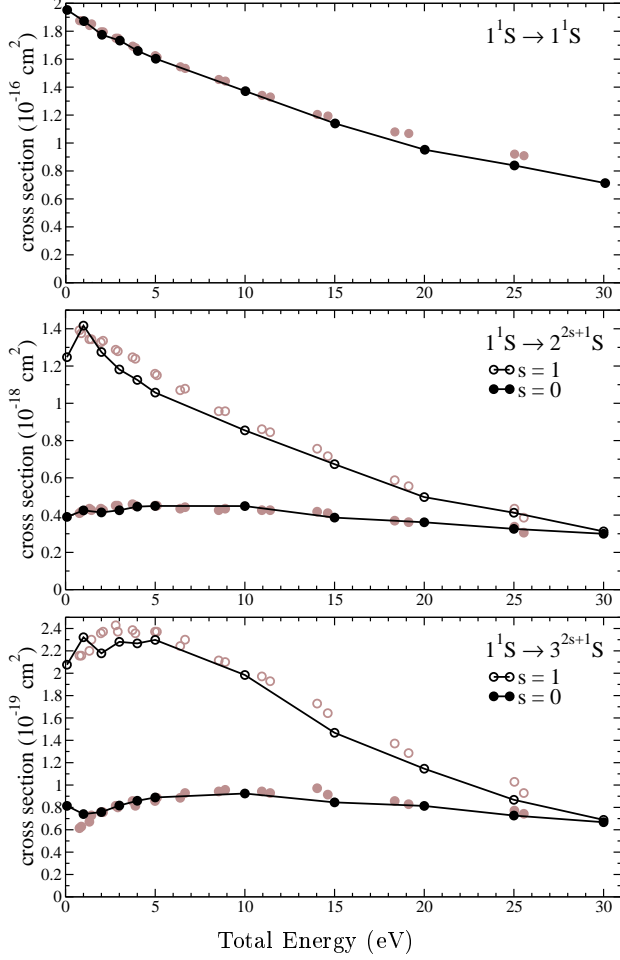


FIG. 1: Excitation cross sections from the 1^1S , ground state. Filled symbols: singlet final states. Open symbols: triplet final states. Symbols with dark lines: Current ECS results. Light symbols: CCC results from [13]

We must emphasize again that these ionization amplitudes, written in Eq. (32) as volume integrals for notational simplicity, must be evaluated as surface integrals. Again, these amplitudes are not completely independent, but related through the following symmetries,

$$\begin{aligned}
f_{fi}^{(1)}(k_1, k_2) &= \pi_i f_{fi}^{(2)}(k_2, k_1) \\
f_{fi}^{(3)}(k_1, k_2) &= \pi_i f_{fi}^{(3)}(k_2, k_1).
\end{aligned}
\quad (33)$$

The “physical” ionization amplitudes $F_{i \rightarrow f}^{S, s_f, s_i}$ are again

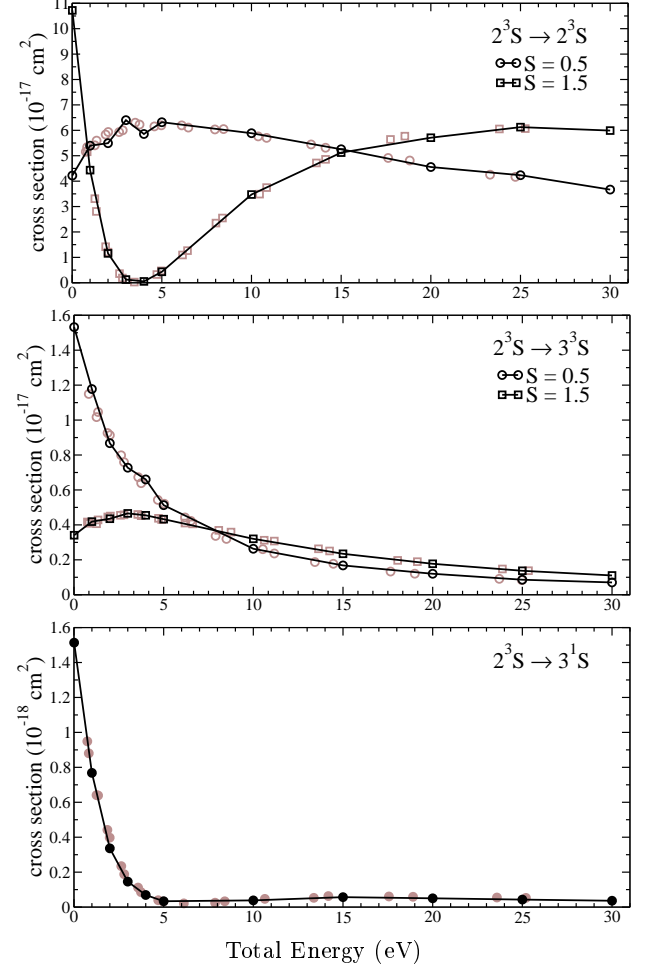


FIG. 2: As in Fig. 1, for the 2^3S , excited state.

given in terms of the arrangement amplitudes in Eq. (32) by the same formulas shown in Table I.

To compute the cross sections for unpolarized incident electrons, we must sum the contributions from all allowed intermediate spin couplings. For overall doublet coupling ($S = 1/2$), the single differential cross sections are given by

$$\begin{aligned}
\frac{d\sigma^{S=1/2}}{d\epsilon} &= \frac{4}{k_1 k_2 E_0} \frac{1}{(2s_i + 1)} \left(\left| F_{fi}^{1/2, s_f=0, s_i}(k_1, k_2) \right|^2 \right. \\
&\quad \left. + \left| F_{fi}^{1/2, s_f=1, s_i}(k_1, k_2) \right|^2 \right),
\end{aligned}
\quad (34)$$

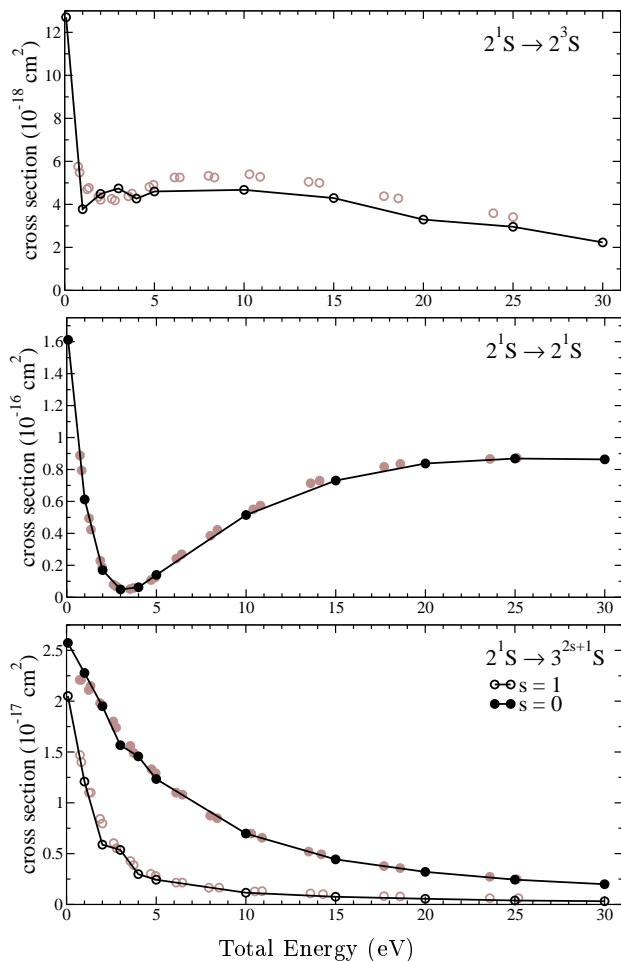


FIG. 3: As in Fig. 1, for the 2^1S excited state.

while for the high-spin case ($S = 3/2$), the cross section is

$$\frac{d\sigma^{S=3/2}}{d\epsilon} = \frac{4}{k_1 k_2 E_0} \left(\frac{2}{3}\right) \left(\left| F_{fi}^{3/2, s_f=1, s_i=1}(k_1, k_2) \right|^2 \right). \quad (35)$$

The total ionization cross section for a given total spin is computed by integrating the SDCS:

$$\sigma^S = \int_0^E \frac{d\sigma^S}{d\epsilon} d\epsilon. \quad (36)$$

III. RESULTS

The computations were all carried out using an FEM-DVR representation of the wave functions for a single initial arrangement on a three-dimensional grid. For each radial dimension, the DVR was based on 15th order Gauss-Lobatto quadrature in each of 11 finite elements, 9 real and 2 complex, for a total of 153 basis functions. The complex turning point, R_0 , was located

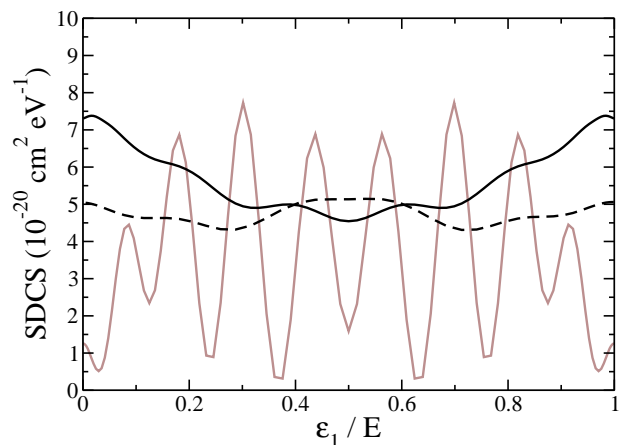


FIG. 4: Comparison of SDCS for ground-state helium at $E = 3$ eV computed with and without the use of distorted waves and/or asymptotic subtraction. Light solid curve: SDCS (divided by 10) obtained with Coulomb functions and no asymptotic subtraction. Dashed curve: SDCS obtained with Coulomb functions and asymptotic subtraction. Dark solid curve: SDCS obtained with distorted waves and asymptotic subtraction.

at 101 bohr. The full three-dimensional grid thus contained $153^3=3,581,580$ points. We have already noted that the DVR gives a diagonal representation of all local operators. In this context, we should point out that an accurate DVR representation of the two-electron repulsion operators that appear in Eqs. (22) and (23) requires some care. These details are fully described in ref. [11]. The time propagation was carried out using the split operator and Crank-Nicolson schemes previously described in section II A. The wave function was evolved in time to $T_{\max} = 400$ a.u with time steps of $\Delta t = 0.1$ a.u.

The amplitudes for excitation and ionization were all assembled from permutations of the appropriate single-arrangement amplitudes, based on final and initial symmetries, as indicated in Table I. These arrangement amplitudes were all evaluated using the surface integral forms of the amplitude expressions, Eqs. (28, 32). The edges of the surface were located just inside R_0 at 100 bohr.

We have calculated excitation and ionization cross sections for the S-wave model from both ground- and excited-state, 2^3S and 2^1S , target atoms. The two-electron target states were always obtained by diagonalizing the target Hamiltonian given in Eq. (23) using the real portion of the 2D FEM-DVR basis.

Figures 1, 2, and 3 show cross sections starting from He 1^1S , 2^3S and 2^1S , respectively, for excitation to states with principle quantum number up to $n = 3$. We have also plotted the results of convergent close coupling (CCC) calculations [13] in those figures for comparison. In all cases, the agreement between the two methods is good. This comparison also indicates that, for excitation, the frozen-core model, which is used in the CCC calculations, and the full model with two active electrons used

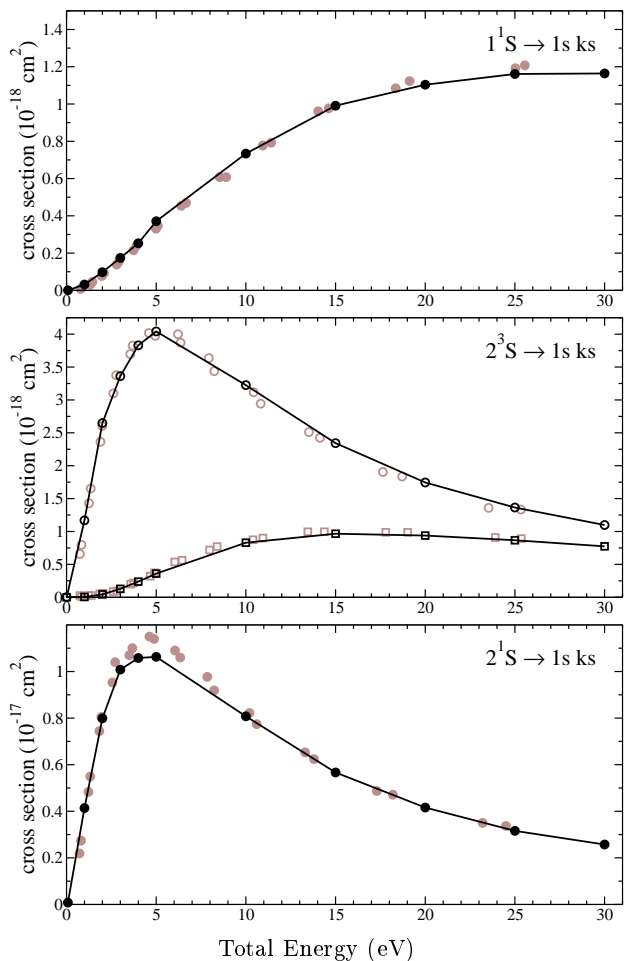


FIG. 5: Total ionization cross sections from different initial states.

here give very similar results.

Differential single ionization cross sections were computed from the ionization amplitude expression given in the previous section. The SDCS were then numerically integrated over the full range of ejected electron energy to produce total ionization cross sections.

As outlined above, the ionization amplitudes were computed using triplet static-exchange distorted waves for the ejected free electrons along with scattered waves in which the ionization component was isolated using asymptotic subtraction. Nine two-body channels, corresponding to target states with principal quantum number up to $n = 5$, were used in the asymptotic subtraction. The use of properly defined distorted waves, as well as asymptotic subtraction, are both critically important in obtaining accurate ionization cross sections. This point is illustrated in Fig. 4, where we show the SDCS for ground-state ionization at $E = 3$ eV computed three different ways, first with Coulomb functions and no asymptotic subtraction, then with Coulomb functions and asymptotic subtraction and finally with distorted waves and asymptotic subtraction.

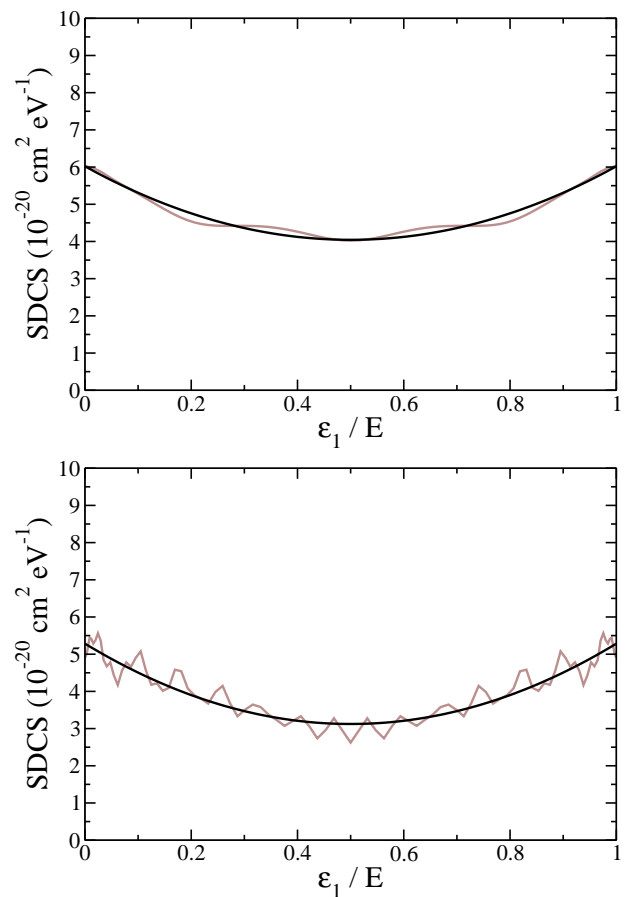


FIG. 6: Examples of SDCS fitting at 2.0 eV (left) and 30.0 eV (right) above the first IP starting in the 1^1S ground state. Dark curve: quadratic fit of SDCS. Light curve: computed SDCS.

The total ionization cross sections from the different initial states are all plotted in Fig. 5, along with the frozen-core CCC results [13]. Once again, we find very good agreement with the CCC results. There is a slight discrepancy in the case of ionization starting in the 2^1S state, where the present total cross sections peak at slightly smaller values than the CCC results.

The single differential cross sections offer the most detailed information about breakup in the S-wave model and are the most difficult quantities to accurately calculate. Even with asymptotic subtraction and the properly chosen distorted waves there are small oscillations in the cross sections, which arise from incomplete elimination of excited singlet two-body states, which are not completely orthogonal to the distorted wave. Fig. 6 shows the SDCS from the ground-state at total energies of 2 and 30 eV, to show the typical behavior at low and high energies. We found that the SDCS in all cases could be well fit with a quadratic function whose parameters are uniquely determined by a least-squares fit that gives the same integrated cross sections as the unsmoothed data. The SDCS values presented in Figs. 7-10 are all obtained

from the fitted quadratic curves.

Interestingly, the SDCS for the high spin, $S = 3/2$, case, shown in Fig. 9, required no smoothing at all. The scattered waves which determine these cross sections, by symmetry, can only contain contributions from triplet two-body channels. The triplet distorted waves we employ remove these contributions effectively exactly. We verified that for these cases, identical results are obtained without asymptotic subtraction. We note that the high-spin SDCSs are zero at equal-energy sharing, which is also required by symmetry.

Differences between the present S-wave results and the frozen-core CCC treatment become more apparent when we compare SDCS values. In the CCC study, SDCS results are only reported for equal-energy sharing, for which case CCC is purported to provide convergent results [13, 22]. In Fig.11, the SDCS, at equal-energy sharing, are plotted as a function of total energy. Since Plottke *et al.* define the total cross section as the integral of the SDCS from zero to $E/2$, we have multiplied our results by two for the comparison. Also, the CCC results were published as separate singlet and triplet contributions, not as their sum. However, the triplet contribution to the SDCS at equal energy sharing should, formally, be 3 times the singlet contribution. Thus to compare with our results, we have multiplied the CCC singlet contributions by 4, and the triplet contributions by 4/3. While the present results and the CCC values are in good agreement above 10 eV, the CCC SDCS are noticeably smaller at lower energies.

IV. DISCUSSION

This study represents a first step in applying the ECS formalism to treat electron collisions with a target that has two active electrons. The S-wave model, which simplifies the full e^- -He problem by treating only states with zero angular momentum, is nevertheless a true Coulomb four-body problem and, when treated in full dimensionality, displays much of the complexity of the full problem. By employing a time-dependent formulation of exterior complex scaling, we can still obtain a numerical repre-

sentation of the time-independent scattered wave while avoiding the problem of solving large systems of complex linear equations. There is therefore every reason to believe that the same numerical techniques we have used in this study could be successfully applied to the full e^- -He problem.

The amplitudes for discrete excitation are easily computed from the numerically obtained scattered waves and are found to give cross sections that agree well with previous CCC studies that employed a frozen-core model. The calculation of accurate ionization amplitudes, on the other hand, poses significant formal and computational difficulties that are not encountered when dealing with single active electron targets. Our approach to this problem has been to combine ‘‘asymptotic subtraction’’ along with a judicious choice of continuum distorted waves to minimize the contamination of the ionization amplitudes by discrete two-body channels. This strategy was found to be reasonably successful in the present case and should also carry over to the full e-He problem. While the total cross sections for ionization we computed were found to agree well with the frozen-core CCC results, there were noticeable differences in the single differential cross sections, particularly at low energies. It is not clear whether these differences can be attributed to deficiencies in the frozen-core model or to convergence problems in the CCC calculations.

Acknowledgments

The authors acknowledge valuable discussions with Wim Vanroose on various numerical aspects of time-propagation. This work was performed under the auspices of the US Department of Energy by the University of California Lawrence Berkeley National Laboratory under Contract DE-AC03-76SF00098 and was supported by the U.S. DOE Office of Basic Energy Sciences, Division of Chemical Sciences. The calculations were carried out at the National Energy Research Scientific Computing Center at Lawrence Berkeley National Laboratory. DAH acknowledges support from the U.S. DOE Computational Science Graduate Fellowship Program.

-
- [1] C. W. McCurdy, M. Baertschy, and T. N. Rescigno, *J. Phys. B* **XX**, xxxx (2004).
 - [2] R. K. Peterkop, *Opt. Spectrosc.* **13**, 87 (1962).
 - [3] M. R. H. Rudge and M. J. Seaton, *Proc. Roy. Phys. Soc.* **283**, 262 (1965).
 - [4] M. R. H. Rudge, *Rev. Mod. Phys.* **40**, 564 (1968).
 - [5] M. S. Pindzola and D. R. Schultz, *Phys. Rev. A* **53**, 1525 (1996).
 - [6] M. S. Pindzola and F. Robicheaux, *Phys. Rev. A* **54**, 2142 (1996).
 - [7] L. Malegat, P. Selles, and A. K. Kazansky, *Phys. Rev. Lett.* **85**, 4450 (2000).
 - [8] C. W. McCurdy, T. N. Rescigno, and D. Byrum, *Phys. Rev. A* **56**, 1958 (1997).
 - [9] M. Baertschy, T. N. Rescigno, W. A. Isaacs, X. Li, and C. W. McCurdy, *Phys. Rev. A* **63**, 022712 (2001).
 - [10] M. Baertschy, T. N. Rescigno, and C. W. McCurdy, *Phys. Rev. A* **64**, 022709 (2001).
 - [11] C. W. McCurdy, D. A. Horner, and T. N. Rescigno, *Phys. Rev. A* **65**, 042714 (2002).
 - [12] M. S. Pindzola, D. Mitnik, and F. Robicheaux, *Phys. Rev. A* **59**, 4390 (1999).
 - [13] C. Plottke, I. Bray, D. V. Fursa, and A. T. Stelbovics, *Phys. Rev. A* **65**, 032701 (2002).

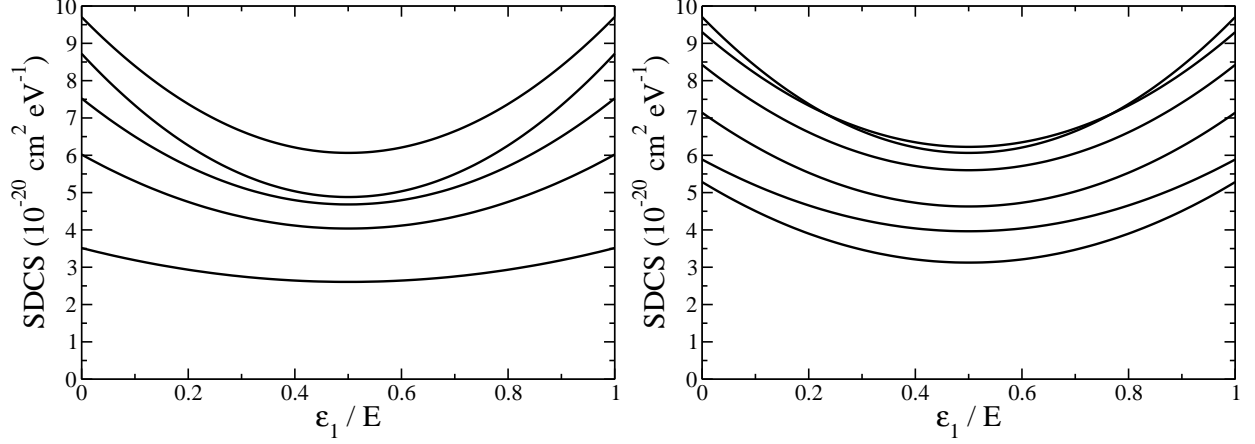


FIG. 7: SDCS for ionization from the 1^1S ground state for various energies above the first IP. Left panel, top to bottom: 5.0, 4.0, 3.0, 2.0 and 1.0 eV. Right panel, y-axis intercept from top to bottom: 5.0, 10.0, 15.0, 20.0, 25.0 and 30.0 eV

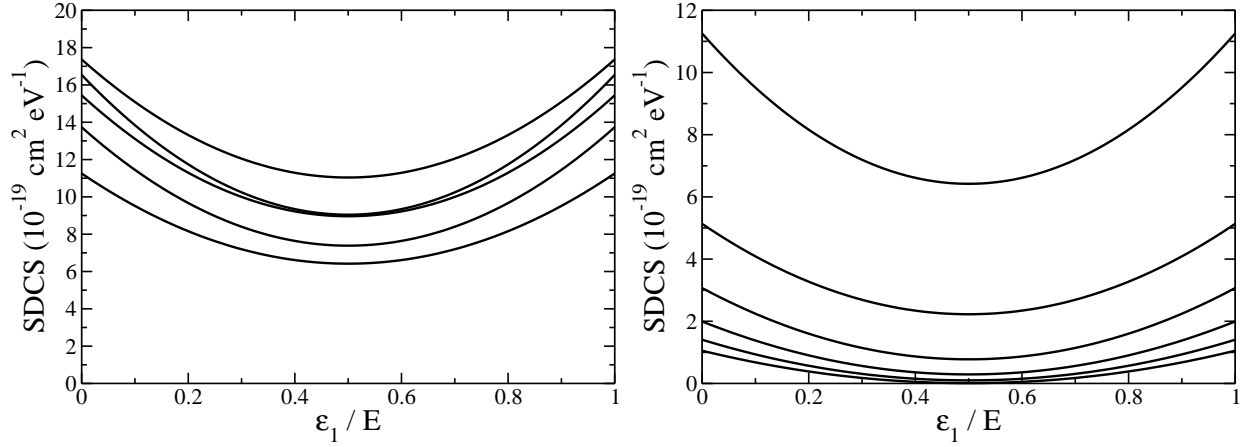


FIG. 8: SDCS for ionization from the 2^3S ground state for various energies above the first IP, with $S = 1/2$. Left panel, top to bottom: 2.0, 1.0, 3.0, 4.0 and 5.0 eV. Right panel, top to bottom: 5.0, 10.0, 15.0, 20.0, 25.0 and 30.0 eV

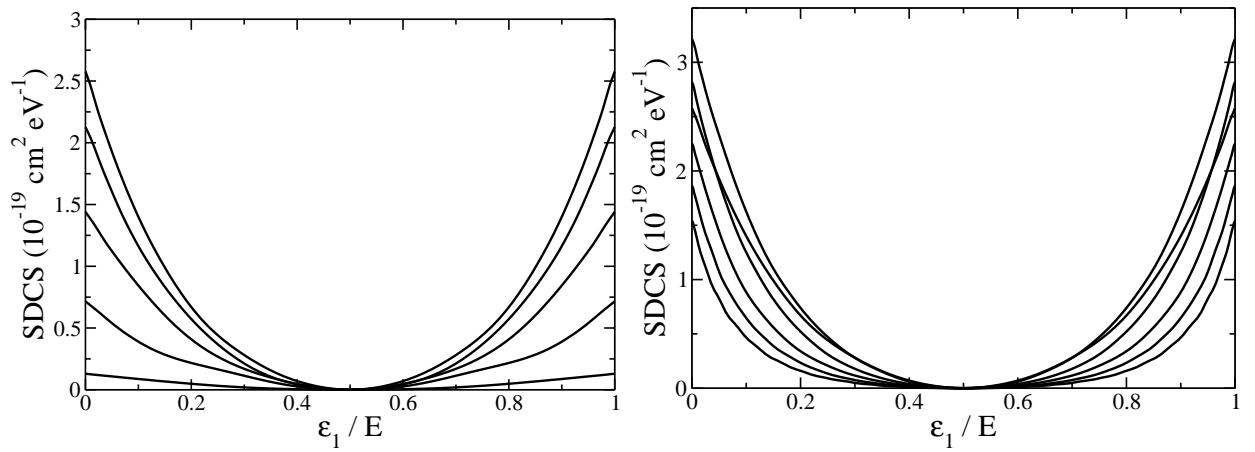


FIG. 9: SDCS for ionization from the 2^3S ground state for various energies above the first IP, with $S = 3/2$. Left panel, top to bottom: 5.0, 4.0, 3.0, 2.0 and 1.0 eV. Right panel, y-axis intercept from top to bottom: 10.0, 15.0, 5.0, 20.0, 25.0 and 30.0 eV

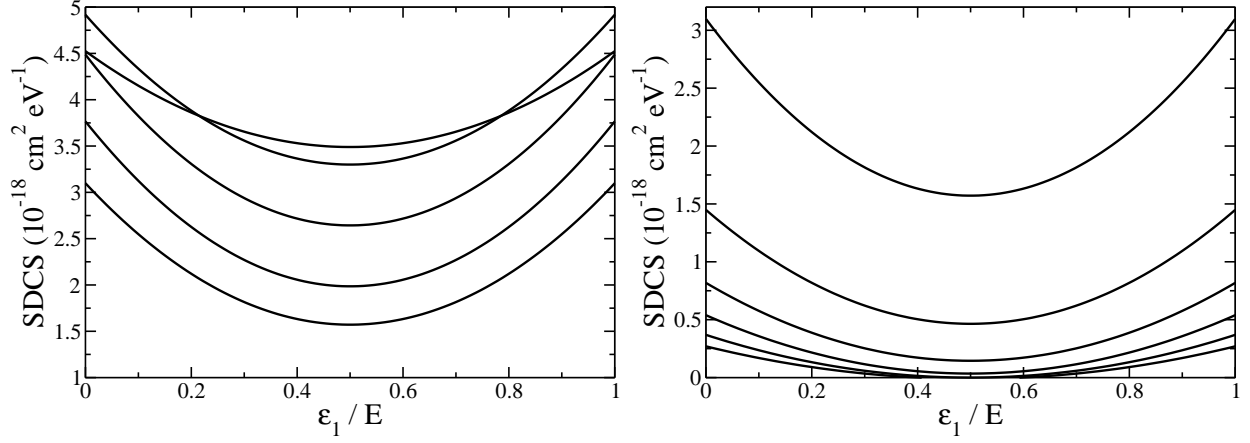


FIG. 10: SDCS for ionization from the 2^1S ground state for various energies above the first IP. Left panel, y-axis intercept from top to bottom: 2.0, 1.0, 3.0, 4.0 and 5.0 eV. Right panel, top to bottom: 5.0, 10.0, 15.0, 20.0, 25.0 and 30.0 eV

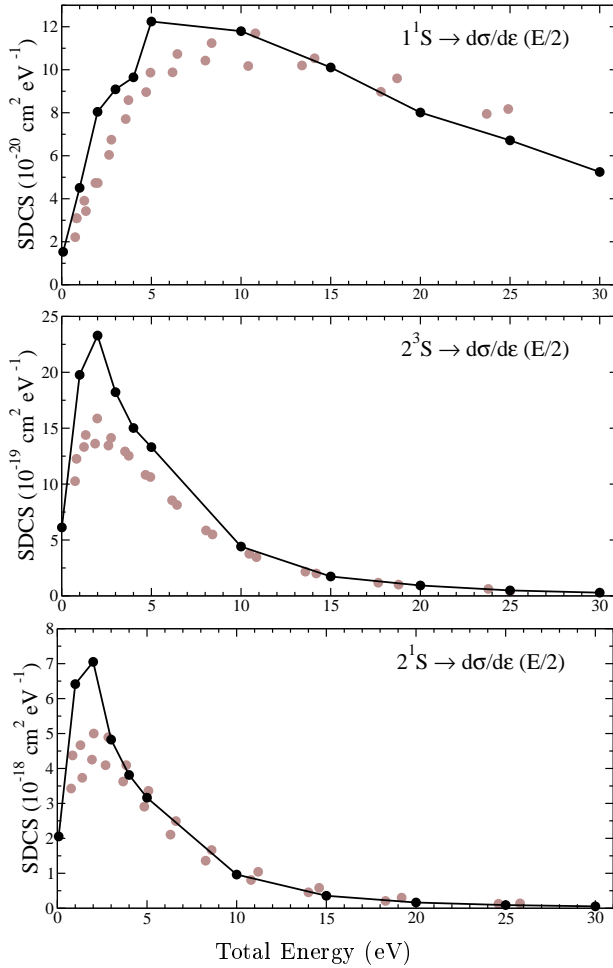


FIG. 11: Single differential cross sections at equal energy sharing for initial states (top to bottom) 1^1S , 2^3S , 2^1S in the case of $S = 1/2$. Dark lines: Current ECS results multiplied by 2.0. Light points: CCC results from [13] scaled as explained in text.

- [14] T. N. Rescigno and C. W. McCurdy, Phys. Rev. A **62**, 032706 (2000).
- [15] C. W. McCurdy and T. N. Rescigno, Phys. Rev. A **62**, 032712 (2000).
- [16] C. W. McCurdy, D. A. Horner, and T. N. Rescigno, Phys. Rev. A **63**, 022711 (2001).
- [17] T. N. Rescigno, M. Baertschy, D. Byrum, and C. W. McCurdy, Phys. Rev. A **55**, 4253 (1997).
- [18] M. D. Feit, J. D. F. Jr., and A. Steiger, J. Comp. Phys. **47**, 412 (1982).
- [19] D. E. Manolopoulos and R. E. Wyatt, Chem. Phys. Lett. **152**, 23 (1988).
- [20] T. N. Rescigno, M. Baertschy, W. A. Isaacs, and C. W. McCurdy, Science **286**, 2474 (1999).
- [21] T. N. Rescigno, M. Baertschy, and C. W. McCurdy, Phys. Rev. A **68**, 020701 (2003).
- [22] I. Bray, Phys. Rev. Lett. **78**, 4721 (1997).